Waves & Oscillations in the Solar Atmosphere:
Heating and Magneto-Seismology
Proceedings IAU Symposium No. 247, 2007
R. Erdélyi & C. A. Mendoza-Briceño, eds.

doi:10.1017/S1743921308015044

Overview of XRT performance and first results

Antonia Savcheva[1] and the XRT Team

[1]Harvard-Smithsonian Center for Astrophysics, 60 Garden st, Cambridge, MA02139, USA
email: asavcheva@cfa.harvard.edu

Abstract. In this review we present a short introduction to the X-ray Telescope on Hinode. We discuss its capabilities and new features and compare it with Yohkoh SXT. We also discuss some of the first results that include observations of X-ray jets in coronal holes, shear change in flares, sigmoid eruptions and evolution, application of filter ratios and differential emission measure analysis, structure of active regions, fine structure of X-ray bright points, and modeling non-potential fields around filaments. Finally, we describe how XRT works with other ground and space-based instrumentation, in particular with TRACE, EIS, SOT, and SOLIS.

Keywords. instrumentation: detectors, instrumentation: high angular resolution, Sun: corona, Sun: magnetic fields

1. Introduction

The X-ray Telescope (XRT) on board the Hinode mission is a collaborative effort between the American side - SAO, and the Japanese side - JAXA and NAOJ. The contribution of SAO was building the mirror, the filter wheel and filters, as well as the structure and mechanical systems. JAXA and NAOJ designed and manufactured the camera sensor and electronics, and the MDP software interface. The mission was launched on 27 Sep 2006 and since November 2006 it has been constantly acquiring scientific data, most of the time in coordinated campaigns with other space and ground-based instruments. Extensive campaigns concentrating on polar coronal holes, dynamics in active regions and X-ray bright points have been conducted. The success of these studies was possible because of the unique combination of characteristics of the telescope, which currently makes it the best X-ray telescope for studying the Sun in orbit.

2. XRT Overview

2.1. *Capabilities and New Features*

XRT is a modified Wolter I telescope with a 35 cm aperture and a 2.71 m focal length. In Fig. 1 you can see a general view of Hinode. The particularly high sensitivity of the telescope is achieved by using a low thermal noise CCD and a low scattering mirror. In addition, XRT has the opportunity for on-orbit focus adjustment and provides a flare flag to alert other instruments observing in parallel. Since the focus is not uniform over the field of view but is best on the optical axis, the focus adjustment capability allows for best on axis imaging of small FOV or optimized imaging across a wide FOV. In addition, XRT has the ability to conduct flexible operations: Automatic Exposure Control (AEC) for automatically choosing the most suitable exposure time to match the changing conditions on the Sun; Flare Detection (FD) images for monitoring the full disk for flares; Pre-Flare buffer to buffer pre-flare images just before the flare for further analysis. XRT has the

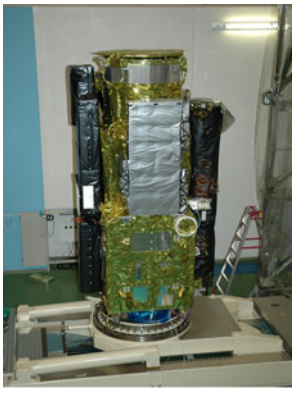

Figure 1. A view on the Hinode spacecraft. The tube in the middle is the SOT, attached to the left is EIS, and on the right is XRT

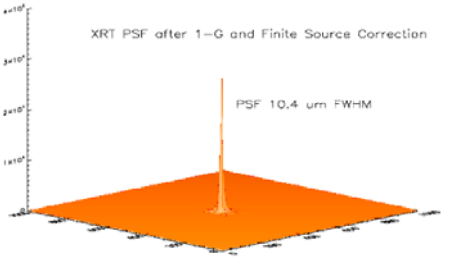

Figure 2. A representation of the XRT PSF as measured at the X-ray calibration facility in Hindsville, Alabama.

ability to conduct high cadence observations of partial FOV, e.g. 512"x512" images every 30s or less (memory usage taken into account) or full sun images every 2min.

The basic property that makes XRT so unique which is basic for understaning and using XRT, is its unprecedented angular resolution of 1 arcsec/pixel. This is 2.5-5 times higher spatial resolution than Yohkoh/SXT - when taking full disk images Yohkoh had to bin the data 2 times. This resolution is achieved by the extremely low scattering mirror which gives a very well defined PSF. As it is evident from Fig. 2 the PSF has a very well defined core as well as very low scattering wings. The encircled energy of the PSF is 68 % within a 2 arcsec diameter circle at 0.523 KeV.

Another very important feature of XRT is its improved temperature sensitivity over a broader range of 1-50 MK. The broad temperature coverage is utilized by the use 9 filters and a high-quality, low-noise, back-thinned 2048x2048 CCD. The filters are arranged in 2 filter wheels (Fig. 3). By rotating the filter wheels we can take images either in one filter, make different filter combinations, or take visible light images for alignment with other instruments. In December 2006 - January 2007, we could not use FW1, but since then both filter wheels have been fully operational. There are three types of filters depending on their optical transmissivity - thin, medium and thick. In Fig. 4 are shown the temperature response curves of all filters and some thin filter combinations. As it can be seen the curves very well cover the temperature-signal plane. The curves demonstrate that the thin filters cover lower temperatures and the thick ones are cut off at theese temperatures. In principle, when observing 10^7K plasma, by only changing the exposure time one should be able to obtain scientific images in thin as well as thick

https://doi.org/10.1017/S1743921308015044 Published online by Cambridge University Press

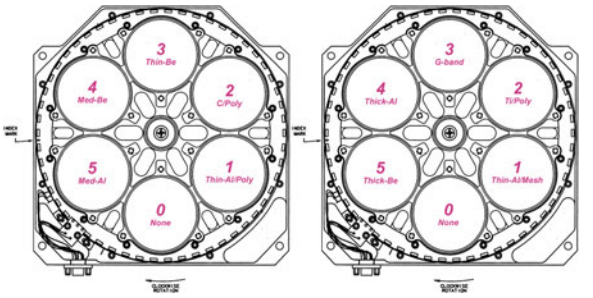

Figure 3. A view on filter wheels 1 and 2 with positions of the filters and the G-band

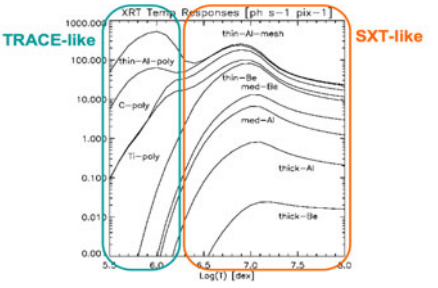

Figure 4. Temperature response curves for all filters and some filter combinations.

filters. The number of different filters, and in particular their different low-temperature cutoff allows for finer temperature discrimination when using filter ratios or differential emission measure analysis.

2.2. *Comparison with Yohkoh*

It is useful and enlightening to compare XRT with previous grazing incidence telescopes in order to better appreciate the unique features of XRT. In particular, we compare it with Yohkoh/SXT since this telescope was widely used by many solar physicists and was a pioneer in studying many X-ray phenomena on the Sun. On Fig. 5 we have shown two typical XRT and SXT images. The XRT image is a full resolution full disk image obtained by combining a short (0.5s) and a long (4s) exposures. That way both faint details in the quiet Sun and the bright features in the active region are well visible. The image is also scaled logarithmically so that the 10^4 dynamic range is well displayed. As it can be seen from the figure XRT does much better job at seeing the faint parts of the Sun because of its coverage at low temperatures - XRT goes to lower temperatures than Yohkoh did. The boundaries of the coronal holes are also much better resolved and identified. In the same time the core and the outskirts of the active region are also much better resolved than with SXT. This is so because of the good temperature response to high temperatures in combination with the 5 times better spatial resolution. Both the high-temperature core of the active region as well as the lower temperature outer parts are resolved to loops. This way, XRT demonstrated that high-temperature plasma is no inherently fuzzy as it was thought before. The highly improved angular resolution also plays a huge role in resolving the structure of X-ray bright points (XBPs). Yohkoh got the credit for discovering the XBPs but XRT showed for the first time that XBPs are composed of loop-like structures and they are not some amorphous blobs of X-ray emission.

In addition to the highly increased angular resolution and better temperature coverage, XRT has better temporal resolution supplied mainly by the greater on-board memory and

https://doi.org/10.1017/S1743921308015044 Published online by Cambridge University Press

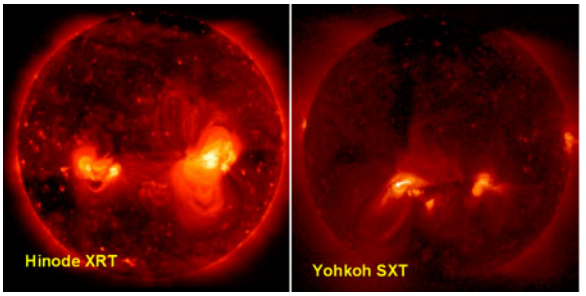

Figure 5. Comparison between Hinode XRT (left) and Yhkoh SXT (right). The images are taken at similar stage of the solar cycle and are shown to the same scale.

faster data rates. This makes XRT suitable for studying both small topological features as well as highly dynamical phenomena.

3. First Results

In designing XRT, there were three basic ideas of what it would be used for. These ideas translated into three basic observation modes in which XRT operates. Combinations and modifications of these are of course possible depending on the purpose of the observation. The first mode is Dynamics mode, which is meant to study the rapid evolution associated with reconnection and plasma instabilities. This mode is characterized with taking high cadence images, so that the time evolution of different structures is followed. The next mode is the Energetics one, which is used for exploring the emission measure evolution of structures: heating, cooling, and EM changes. To achieve this observations are conducted in multiple filters and filter combinations so that a fine temperature discrimination is achieved. The use of multiple filters, however, means that high-cadence observations in the same filter cannot be made. The third mode of observation is intended to study the topology of different structures and identify the magnetic connections that control the heating and dynamics in these regions. When in this mode large-FOV images are taken usually one with long and one with short exposure. As we mentioned, by combining long and short exposure in one filter, one can make the details in the quiet Sun stand out as well as resolve the core of the active regions to loops. Using these observation modes different analysis techniques were used to bring up the first results of the first ten months of operation of XRT.

3.1. *Statistical Properties of X-ray Jets*

During February and March 2007 the most extensive observational campaign of polar jet formation and evolution from within both the north and south polar coronal holes was conducted by XRT. For the first time, this study showed that X-ray jets in the polar coronal holes occur at very high frequency - about 60 jets/day on average. Using the observations collected by XRT, several physical parameters of a large sample of jets were statistically studied. This work has been done by Antonia Savcheva *et al.* from the XRT group at the Harvard-Smithsonian Center for Astrophysics, Cambridge, USA.

On Fig. 6, we have shown an example of a jet when it has reached its maximum height - the underlying bi-pole structures are well visible. We have also shown the famous cartoon picture by Shibata and Shimojo that depicts the reconnection mechanism that gives rise to the X-ray jet (Fig. 7). Notice the obvious visual resembles.

The apparent outward velocity, the height, width and lifetime of the jets were measured. Since velocities are very important for discriminating between different accelera-

https://doi.org/10.1017/S1743921308015044 Published online by Cambridge University Press

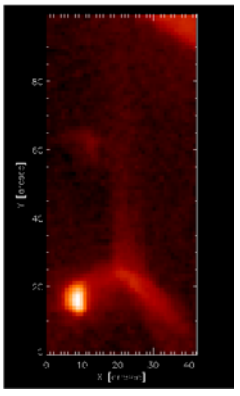

Figure 6. An image of X-ray jet when it has reached its maximum extent. The image is taken in Al_poly filter on 01/17/07 13:11 UT.

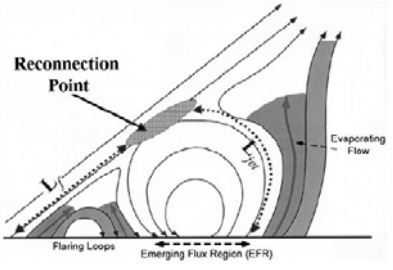

Figure 7. The famous cartoon by Shimojo and Shibata demonstrating the reconnection scenario.

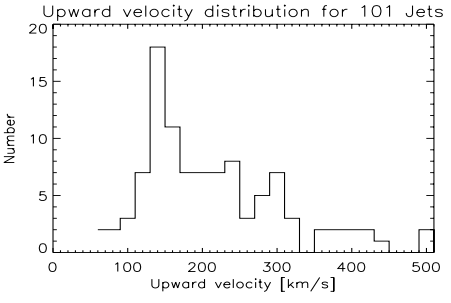

Figure 8. Histogram distribution of jet outward velocities for 101 jets.

tion mechanisms, we have developed four methods for determining the outward apparent velocity of jets. One is based on the following idea: the central vertical rectangle of image is summed across rows to yield a single column; the columns are then placed sequentially side-by-side to produce a time-ordered image; the slope of near-vertical feature gives velocity of outward-moving front. The distribution of velocities for 100 jets (Fig. 8) peaks at 160 km/s, which points to the possibility of evaporation flow in the lower corona.

We also plot the positions of all jets atop the boundary of the polar coronal hole and show that, despite some possible selection effects, jets preferably occur inside the polar coronal holes. It is still not entirely clear whether this is due to the fact that jets indeed occur rarely when embedded in closed magnetic field or it is just harder to observe them,

https://doi.org/10.1017/S1743921308015044 Published online by Cambridge University Press

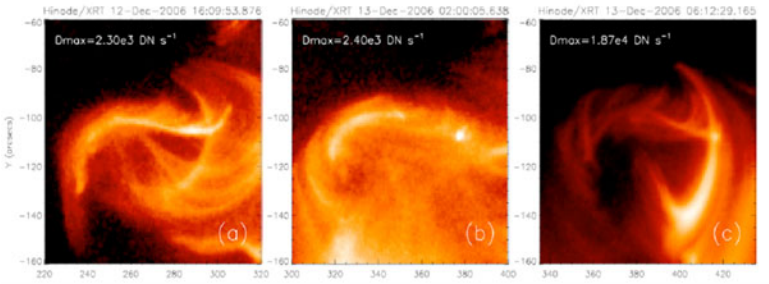

Figure 9. XRT flare loops from December 13, 2006 in pre-flare phase (right and center) and post-flare phase (left). Notice that the shear in the loops has been reduced during the flare.

but for sure it has to do with the fact that the global field changes configuration from open to close.

3.2. *Shear Magnetic Fields*

Another topic of research, which belong to exploring the topology of magnetic field structures in XRT data is the study of the evolution of sheared magnetic fields in flare loops around filaments. The shear motion of the footpoints of flare loops has been noticed before in TRACE data, where the shear angle has been observed to change 10°-60° from before to after the flare. The assumption that shear is released during the flare and can built up subsequently in order to produce repeated flares has been studied in XRT data, as inspired by previous work on TRACE EUV data. This work has been dome by Yingna Su *et al.* from the XRT group at the Harvard-Smithsonian Center for Astrophysics, Cambridge, USA.

The analysis is done on XRT data from December 13 and 14, 2006, when NOAA active region 10930 produced two X-class flares. Observations showed that stress has been building up in this region as a consequence of the rotation and west-to-east translational motion of the newly forming sunspot. As it can be seen from Fig. 9 the pre-flare loops in the core region appear to be very sheared. XRT observations show that only part of the sheared core erupted and some sheared loops stayed. This is also visible in TRACE data where part of the filament erupted and part of it remained after the flare. It has been noticed that while the core looses its shear during the flare, some time after that the shear builds up again. All this points to the fact that the energy of the flare is initially stored in the highly sheared magnetic fields in the core flare loops.

3.3. *XRT Observations of a Coronal Sigmoid*

Another interesting observation and subsequent analysis is that of a sigmoid formation and eruption that occurred on February 10, 2007. This work has been done by David E. McKenzie and Richard C. Canfield from Montana State University. First the ruling models of sigmoid formation have been considered. The Rust & Kumar and Pevtsov & Canfield model of emerging twisted flux rope provides no useful description of heating mechanism, so it is not considered further. The Titov & Demoulin model of twisted flux rope embedded in ambient field present the possibility that when a flux rope emerges, there are places where the magnetic field is tangential to the photosphere and concave upward. In the same time the Bald Patch Separatrix Surface model (BPSS) predicts a double-j shape with bright points at the top, which is then tested against observations. The Fan & Gibson model of a twisted flux rope embedded in ambient field and current sheet created during kink instability predicts an S-shape for the sigmoid, which is also compared with the observations. On Fig. 10 one can see a graphic representation of the

https://doi.org/10.1017/S1743921308015044 Published online by Cambridge University Press

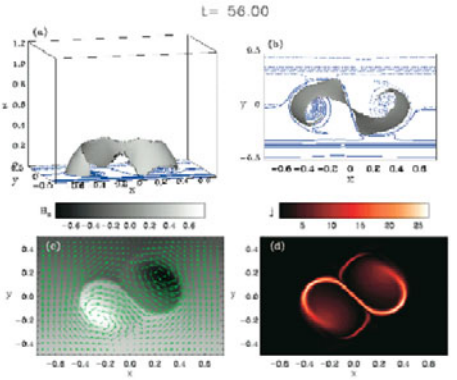

Figure 10. Titov & Demoulin (up) and Fan & Gibson (down) models predictions for the shape of the sigmoid.

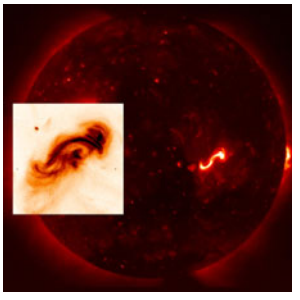

Figure 11. Coronal sigmoid from February 10, 2007.

basic predictions for the size and shape of the emerging sigmoid according to the Titov & Demoulin and Fan & Gibson models.

In Fig. 11 is shown an image of the over-2-days long dataset covering the emergence, evolution and eruption of the sigmoid from February 10, 2007. The whole dataset is taken at a 10-30s cadence which allowed very good study of the time-evolution of the different parts of the sigmoid. For instance, tracking best-guess location of BPs showed that the separation increases with about 26 Mm in 40 hours. Also, tracking the greatest extent of sigmoid "elbows" showed that the overall length increased with approximately 64 Mm in 40 hours.

Some of the key results for the sigmoid shape is that the data matches the prediction of the BPSS model (specifically, the "2-j" shape). And the observations of the sigmoid growth and evolution is consistent with emergence of a twisted flux rope from beneath the photosphere. Sigmoid eruption matches the rotation of bar-shaped ejected feature, which is the prediction of a kinking flux rope. The location of the arcade matches prediction of BPSS model.

3.4. *Temperature Maps and Schmelz AR DEM Analysis*

Resolving the thermal structure of the corona is essential for understanding the coronal heating mechanisms. As mentioned before the broad temperature coverage and multiple filters allow for fine temperature discrimination. Observations in multiple passbands (focal plane analysis filters) allow temperature determination at every pixel in the image. By forming the hardness ratios between the thinner filters and the thicker filters, we are able to finely resolved the highly thermally structured corona in the active regions.

https://doi.org/10.1017/S1743921308015044 Published online by Cambridge University Press

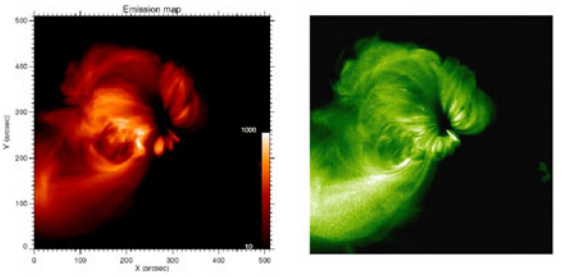

Figure 12. Emission (left) and temperature (right) maps of an active region produced from 5 different filters.

Optimized rations for increasing the signal-to-noise have been devised by Fabio Reale *et al.* from INAF, Palermo, Italy.

As it is evident from Fig. 12 (left), we see numerous fine, hot threads in the active region as well as the cooler outer structure. Nearby large-scale loops seem to have high temperatures, not as usually accepted that the large loops are cool. Comparing the emission and thermal map of the AR shows that dense regions are not necessarily hot, they may be cool as well. The thermal distribution along the loops is continuous, but we also see some evidence of interacting structures. The thermal maps are also compared with TRACE data, so that information about the position and structure of cooler details is extracted.

Differential Emission Measure analysis (DEM) is another way to study temperature structure of AR and the quiet sun. DEM analysis has been conducted on the 11 filters/filter combinations data set from 13 May 2007, full disk images. The "best fit" DEM curve reveals that the maximum of the emission is at $\log T = 6.2$, which corresponds to the quiet sun. The curve shows also a superhot component at $\log T = 7.5$, which may point to heating from nanoflares. However, when we produce different datasets with slightly different conditions, inside the error bars, and make 100 realizations of the DEM, this hotter peak loses confidence.

Another application of the DEM analysis is when applied to every pixel of an image to reveal information about the temperature structure of an active region. Kathy Reeves from the XRT group at the Harvard-Smithsonian Center for Astrophysics, Cambridge, USA uses this to look at the thermal evolution of pre-flare loops. In Fig. 13 you can see the result from applying the DEM analysis to every pixel of a region encompassing the post-flare loops, which were visible shortly after the C8.2 flare that occurred on July 7, 2007. The image is binned in temperature space, so that the brightness of a pixel corresponds to the height of the DEM curve at that place. The important result of these DEM maps is that the post-flare loops seem to cool down in the matter of several tens of minutes. If you look at the left portion of the figure, you can see that there is significant signal in the bin 5-10K, while 20 minutes later here is no signal in that bin and instead the signal is high in the 3-5K bin.

3.5. *Modeling Non-Potential Magnetic Fields In AR 10930*

Filaments, or prominences, are thought to be embedded in highly sheared and/or twisted magnetic structures in the low corona above the polarity inversion line. Active region filaments often have long parallel strands, suggesting such filaments are embedded in untwisted (or weakly twisted) field. To describe such regions one needs to develop a non-potential magnetic field model. Monica Bobra *et al.* from the XRT group at the Harvard-

https://doi.org/10.1017/S1743921308015044 Published online by Cambridge University Press

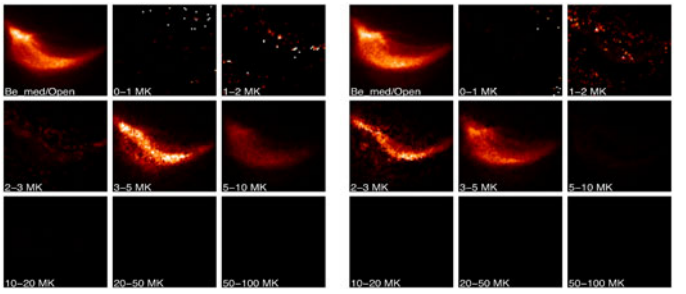

Figure 13. DEM analysis of post-flare loops 10 min after a C8.2 flare (left) and 30min after the flare (right). The data is from July 7, 2007. 7 filters have been used to produce these images. The first bin is the data in Be_med filter and the rest are temperature bins.

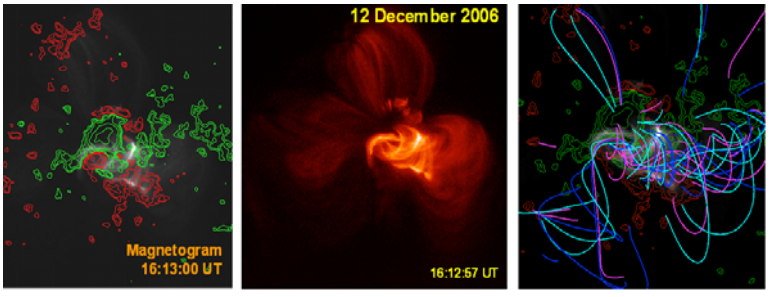

Figure 14. The process of non-potential magnetic field modeling: XRT image with overlaid magnetic field strength contours from Kitt Peak SOLIS (left), XRT image (center) pf NOAA AR 10930, best-fit result from the non-potential magnetic field modeling.

Smithsonian Center for Astrophysics, Cambridge, USA has worked on the different steps one needs in order to develop such a model and match it successfully to the observations.

Modeling the topology and strength of the magnetic field in and around filaments involves constructing a 3D models of the field lines based on observations. Since the corona is a low-β plasma, the magnetic field is close to a non-linear force free field (NLFFF) and constructing a NLFFF involves inserting a "flux rope" into a potential field and allowing relaxation to FF state. Then one constructs a grid of models by varying poloidal and toroidal components of the magnetic field and compare it to observations.

In Fig. 14 we have shown a summary of the steps towards constructing a model of the non-potential field in NOAA active region 10930 from December 12, 2006. One starts with a magnetogram and a H_α image to locate the filament, which is then represented by the "flux rope". By following the above steps and of course keeping an eye on the observations, the model field lines are produced and the best-fit model is chosen. For this particular case the best-fit model has a flux rope with an axial (toroidal) flux value of 10^{21}Mx and poloidal flux value of 10^{11}Mx/cm. It can be seen from the figure that the shape of the field lines qualitatively matches the loops that are seen in the XRT image. Such analysis applied to different stages of a flaring active region, for instance, can give some insight into how the magnetic field reconfigures during a flare.

4. The Play between XRT and Other Instruments

Despite the fact that XRT has many improved and unique characteristics, it is still useful to combine data from XRT and other space- and ground-based instrumentation. An obvious choice of a complementary instrument is TRACE, mostly because it covers

https://doi.org/10.1017/S1743921308015044 Published online by Cambridge University Press

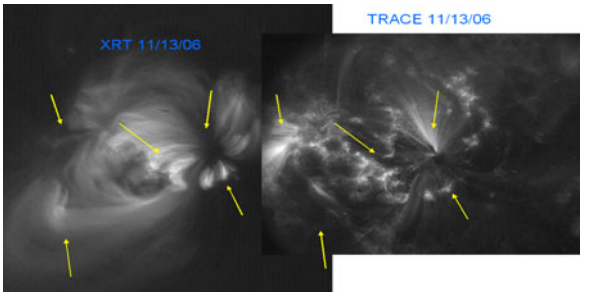

Figure 15. NOAA AR 10923 from November 13, 2006 imaged by XRT (left) and TRACE (right.)

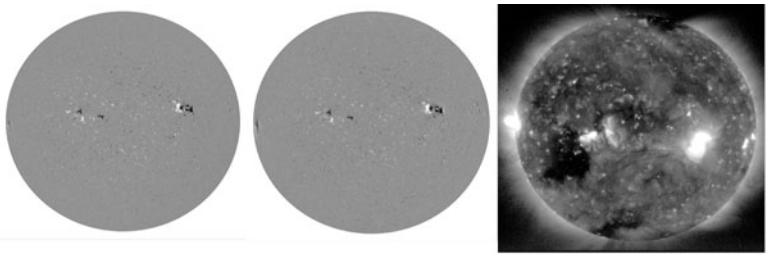

Figure 16. SOLIS photospehric (left) and chromospheric (center) magnetograms, and XRT Al_poly/Ti_poly image (right).

smaller temperatures and hence can image cooler plasma better than XRT. On Fig. 15 one can see a comparison between an XRT and TRACE images of the same active region from the same time. While XRT images well the hot loops, TRACE sees the footpoints of these loops very well. TRACE also observes some cool loops in the outskirts of the active region which are not visible for XRT. These images show an interesting feature - the big bright loop in the left half of the XRT image is not present in the TRACE image which clearly points to the fact that it is actually hot.

Of course, it is natural to combine XRT and the other instruments on Hinode - the Solar Optical Telescope (SOT) and the Extreme Imaging Spectrograph (EIS). The idea is to combine XRT and SOT for photosphere/corona connectivity studies and explore the dynamics and topology of different phenomena at different temperatures and heights in the solar atmosphere. In the same time if XRT is combined with EIS and TRACE to co-observe different eruptive phenomena, like flares for instance, we can get more insight into the energetics and mechanisms of the process.

During the weekly program of EIS 3.5hr disk center calibration, XRT collaborates with the ground-based magnetograph SOLIS. Photospheric vector or LOS magnetograms chomospheric LOS magnetograms are being taken during that time, while XRT runs a multi-filter program of full sun full resolution images. The goals are studies of the relationship of magnetic topology and coronal energetics for quiet sun, active region, and coronal hole. As it can be seen from Fig. 16, one can clearly identify the magnetic structures underneath the active region on the east limb. These magnetograms can be additionally used to run non-potential field models or if taken frequently to identify some time evolution of the magnetic field and connect it with the thermal and topological evolution in the XRT images.

https://doi.org/10.1017/S1743921308015044 Published online by Cambridge University Press

5. Working with Hinode

Chief Coordinators:
John Davis (john.m.davis@nasa.gov)
Tetsuya Watanabe (watanabe@uvlab.mtk.nao.ac.jp).
Science Schedule Coordinators:
SOT: T. Berger (berger@lmsal.com)
XRT: L. Golub (golub@cfa.harvard.edu)
EIS: J. Mariska (mariska@nrl.navy.mil).
XRT Observing (XOB) Proposals: http://solar.physics.montana.edu/HINODE/XRT
XRT USERS Email List: xrt_users-request@head.cfa.harvard.edu

6. Conclusion

XRT is unique X-ray instrument with unprecedented spatial and temporal resolution, which makes it ideal for exploring highly dynamical processes on all kinds of spatial scales. In addition, its broad temperature coverage and multiple filters allow for fine temperature discrimination and studying the energetics of different parts of the sun and separate phenomena. These characteristics determine three main modes of operation - dynamical, topological and energetics. Different studies have been conducted on data taken in these observational modes during the first ten months of operation. Dynamical events, like X-ray jets and flares, have been studied and some interesting results about the statistical properties and magnetic field topologies have been found. Some work on the energetics of the quiet sun and flare loops has been conducted, showing that post-flare loops cool rapidly after a flare. Some numerical modeling of non-potential magnetic fields has also been done based on XRT data and ground-based magnetograms, revealing the magnetic field topology around filaments. Based on these studies some future goals have been set and new topics of investigation have been defined. New observational programs have been developed and XRT continues to provide us with high quality scientific data.

Acknowledgements

Hinode is a Japanese mission developed and launched by ISAS/JAXA, collaborating with NAOJ as a domestic partner, NASA and STFC (UK) as international partners. Scientific operation of the Hinode mission is conducted by the Hinode science team organized at ISAS/JAXA. This team mainly consists of scientists from institutes in the partner countries. Support for the post-launch operation is provided by JAXA and NAOJ (Japan), STFC (U.K.), NASA, ESA, and NSC (Norway).

References

Bobra, M.G., van Ballegooijen, A., DeLuca, E.E., Kano, R., Korreck, K., Narukage, N., Sakao, T., Shibasaki, K., Su, Y. 2007, *PASJ*, accepted

Golub, L., Austin, G., Bookbinder, J., Caldwell, D., Cheimets, P., Cirtain, J., Cosmo, M., DeLuca, E., Reid, P., Sette, A., Weber, M., Sakao, T., Kano, R., Shibasaki, K., McCracken, J., Carpenter, J., Haight, H., Siler, R., Wright, E., Tucker, J., Rutledge, H., Barbera, M., Peres, G., Varisco, S. 2007, *Sol. Phys.* 243, 63

Reale, F., Paraneti, S., Reeves, K., Weber, M., Bobra, M., Barbera, M., Kano, R., Narukage, N., Shimojo, M., Sakao, T., Peres, G., Golub, L. 2007, *Science*, submitted

Savcheva, A., Cirtain, J., DeLuca, E., Lundquist, L., Golub,L., Weber, M., Shimojo, M., Shibasaki, K., Sakao, T., Narukage, N., Tsuneta, S., Kano, R. 2007 *PASJ*, accepted

Su, Y., Golub, L., van Ballegooijen, A., DeLuca, E., Revees, K., Sakao, T., Kano, R., Narukage, N., Shibasaki, K. 2007, *PASJ*, accepted